Brazilian Journal of Physics
ISSN: 0103-9733
luizno.bjp@gmail.com
Sociedade Brasileira de Física
Brasil

Saha, Surajit; Ghosh, Manas
Polarizabilities of Impurity Doped Quantum Dots Under Pulsed Field: Role of Multiplicative White Noise
Brazilian Journal of Physics, vol. 46, núm. 1, febrero, 2016, pp. 41-49
Sociedade Brasileira de Física
São Paulo, Brasil

Braz J Phys (2016) 46:41–49
DOI 10.1007/s13538-015-0380-5

SOCIEDADE BRASILEIRA DE FÍSICA

CONDENSED MATTER

Polarizabilities of Impurity Doped Quantum Dots Under Pulsed Field: Role of Multiplicative White Noise

Surajit Saha[1] · **Manas Ghosh**[2]

Received: 13 March 2015 Published online: 6 November 2015

Abstract We perform a rigorous analysis of the profiles of a few diagonal and off-diagonal components of linear (α_{xx}, α_{yy}, α_{xy}, and α_{yx}), first nonlinear (β_{xxx}, β_{yyy}, β_{xyy}, and β_{yxx}), and second nonlinear (γ_{xxxx}, γ_{yyyy}, γ_{xxyy}, and γ_{yyxx}) polarizabilities of quantum dots exposed to an external pulsed field. Simultaneous presence of multiplicative white noise has also been taken into account. The quantum dot contains a dopant represented by a Gaussian potential. The number of pulse and the dopant location have been found to fabricate the said profiles through their interplay. Moreover, a variation in the noise strength also contributes evidently in designing the profiles of above polarizability components. In general, the off-diagonal components have been found to be somewhat more responsive to a variation of noise strength. However, we have found some exception to the above fact for the off-diagonal β_{yxx} component. The study projects some pathways of achieving stable, enhanced, and often maximized output of linear and nonlinear polarizabilities of doped quantum dots driven by multiplicative noise.

Keywords Quantum dot · Impurity · Polarizability · Pulsed field · Dopant location · Multiplicative white noise · Noise strength

✉ Manas Ghosh
pcmg77@rediffmail.com

[1] Department of Chemistry, Bishnupur Ramananda College, Bishnupur, Bankura 722122, West Bengal, India

[2] Department of Chemistry, Physical Chemistry Section, Visva Bharati University, Santiniketan, Birbhum 731235, West Bengal, India

1 Introduction

The nonlinear optical effects displayed by quantum dots (QDs) comprise of rich subtleties, most often even more than the bulk materials. As a result, QDs are used without any hesitation in a wide variety of optical devices. Often, QDs contain dopants thereby causing immense change in its properties. The change originates from the interplay between the intrinsic dot confinement potential and the introduced dopant potential. Such a change in the dot properties has led to a number of prominent investigations on doped QD [1–9]. In the context of optoelectronic applications, impurity-induced modulation of linear and nonlinear optical properties is highly important in photodetectors and in several high-speed electro-optical devices [10]. Naturally, researchers have worked a lot on both linear and nonlinear optical properties of these structures [10–31].

External electric field often illuminates important features that originate because of the confined impurities. The electric field invariably modifies the spatial disposition of the energy levels of the carrier and thus affects the performance of the optoelectronic devices. In addition, the electric field hampers the spatial symmetry of the system to various extents and promotes emergence of nonlinear optical properties. Thus, the applied electric field deems special importance in the field of research on the optical properties of doped QDs [32–48].

Recently, we have made detailed investigations of the role of noise on the linear and nonlinear polarizabilities of impurity doped QDs [49–51]. In the present work, we have explored some of the diagonal and off-diagonal components of linear (α_{xx}, α_{yy}, α_{xy}, and α_{yx}), second-order (β_{xxx}, β_{yyy}, β_{xyy}, and β_{yxx}), and third-order (γ_{xxxx}, γ_{yyyy}, γ_{xxyy}, and γ_{yyxx}) polarizabilities of quantum dots in the presence of Gaussian white noise incorporated multiplicatively to the system. The doped system is exposed to an external pulsed electric field. The diagonal and off-diagonal components are expected to behave in different

manners because of their diverse interactions with the pulsed field and noise. We have found that the number of pulses of the external field (n_p) and the dopant coordinate (r_0) play an important role in shaping the various polarizability components. Added to this, a variation in the noise strength (μ) also influences the said components. A change in n_p in effect changes the amount of energy delivered to the doped system. And the role of dopant site has been given special emphasis following the important works of Karabulut and Baskoutas [25], Baskoutas et al. [32], and Khordad and Bahramiyan [30] from the perspective of optical properties of doped heterostructures. The present inquiry advocates the important roles played by n_p, r_0, and μ in fabricating the various polarizability components in the presence of multiplicative white noise.

2 Method

The Hamiltonian describing a 2-D quantum dot with single-carrier electron laterally confined (parabolic) in the $x-y$ plane and doped with a Gaussian impurity is given by

$$H_0 = H_0^{'} + V_{\text{imp}}, \tag{1}$$

where $H_0^{'}$ is the Hamiltonian in the absence of impurity. Under the effective mass approximation it reads

$$H_0^{'} = \frac{1}{2m^*}\left[-i\hbar\nabla + \frac{e}{c}A\right]^2 + \frac{1}{2}m^*\omega_0^2\left(x^2+y^2\right) \tag{2}$$

The confinement potential is given by $V(x,y) = \frac{1}{2}m^*\omega_0^2$ (x^2+y^2) with the harmonic confinement frequency ω_0 and the effective mass m^*. The value of m^* has been chosen to be $0.067m_0$ resembling *GaAs* quantum dots. We have set $\hbar=e=m_0=a_0=1$ and perform our calculations in atomic unit. The parabolic confinement potential has been utilized in the study of optical properties of doped QDs by Ç akir et al. [17, 19]. Recently, Khordad and his coworkers introduced a new type of confinement potential for spherical QD's called Modified Gaussian Potential (MGP) [52, 53]. A perpendicular magnetic field ($B\sim mT$) provides an additional confinement. In Landau gauge [$A=(By,\ 0,\ 0)$] (A being the vector potential), the Hamiltonian transforms to

$$H_0^{'} = -\frac{\hbar^2}{2m^*}0\left(\frac{\partial^2}{\partial x^2}+\frac{\partial^2}{\partial y^2}\right) + \frac{1}{2}m^*\omega_0^2x^2 + \frac{1}{2}m^*\left(\omega_0^2+\omega_c^2\right)y^2 - i\hbar\omega_c y\frac{\partial}{\partial x}, \tag{3}$$

$\omega_c = \frac{eB}{m^*c}$ being the cyclotron frequency and $\Omega^2=\omega_0^2+\omega_c^2$ represents the effective frequency in the y-direction. V_{imp} being the impurity (dopant) potential (Gaussian) [54, 55] and is given by

$$V_{\text{imp}} = V_0 e^{-\xi\left[(x-x_0)^2+(y-y_0)^2\right]}. \tag{4}$$

Positive values of ξ and V_0 indicate a repulsive impurity. V_0, $(x_0; y_0)$, and ξ^{-1} represent the impurity potential, the dopant coordinate, and the spatial stretch of impurity, respectively.

We have employed a variational recipe to solve the time-independent Schrödinger equation, and the trial function $\psi(x, y)$ has been constructed as a superposition of the product of harmonic oscillator eigenfunctions $\phi_n(px)$ and $\phi_m(qy)$ respectively, as

$$\psi(x,y) = \sum_{n,m} C_{n,m}\phi_n(px)\phi_m(qy), \tag{5}$$

where $C_{n,m}$ are the variational parameters and $p = \sqrt{\frac{m^*\omega_0}{\hbar}}$ and $q = \sqrt{\frac{m^*\Omega}{\hbar}}$. In the linear variational calculation, requisite number of basis functions has been exploited after performing the convergence test. And H_0 is diagonalized in the direct product basis of harmonic oscillator eigenfunctions.

The external pulsed field can be represented by

$$\varepsilon(t) = \varepsilon(0)S(t)\sin(\nu t). \tag{6}$$

$\varepsilon(t)$ is the time-dependent field intensity modulated by a pulse-shape function $S(t)$ where the pulse has a peak field strength $\varepsilon(0)$, and a fixed frequency ν. The pulsed field is applied along both x and y directions. In the present work, we have invoked a sinusoidal pulse given by

$$S(t) = \sin^2\left(\frac{\pi t}{T_p}\right), \tag{7}$$

where T_p stands for *pulse duration time*. Thus T_p, or equivalently np (*the number of pulses*), appears to be a key control parameter. Figure 1 depicts the profiles of five consecutive sinusoidal pulses as a function of time. With the application of pulsed field, the time dependent Hamiltonian becomes

$$H(t) = H_0 + V_1(t), \tag{8}$$

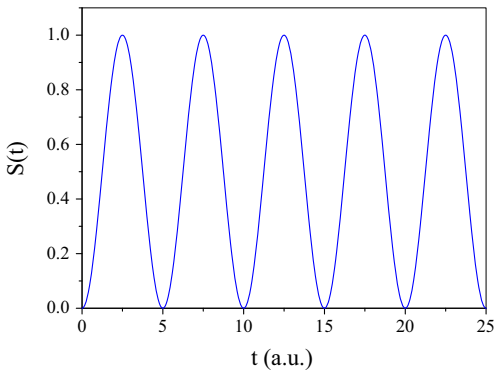

Fig. 1 The sinusoidal pulse profile

where

$$V_i(t) = -|e|\left[\varepsilon_x(t).x + \varepsilon_y(t).y\right] \tag{9}$$

In the presence of multiplicative white noise, the time-dependent Hamiltonian becomes

$$H(t) = H_0 + V_1(t) + V_2(t), \tag{10}$$

with $V_2(t)=\sigma(t)\,(x+y)$, where $\sigma(t)$ is the noise term that follows a Gaussian distribution with characteristics [49, 51]:

$$\langle\sigma(t)\rangle = 0, \tag{11}$$

and

$$\langle\sigma(t)\sigma(t')\rangle = 2\mu\delta(t-t'), \tag{12}$$

where μ stands for the noise strength.

The evolving wave function can now be described by a superposition of the eigenstates of H_0, i.e.,

$$\psi(x,y,t) = \sum_q aq(t)\ \ \psi_q. \tag{13}$$

The time-dependent Schrödinger equation (TDSE) carrying the evolving wave function has now been solved numerically by 6th order Runge-Kutta-Fehlberg method with a time step size Δt=0.01 a.u. after verifying the numerical stability of the integrator. The time-dependent superposition coefficients $[a_q\,(t)]$ has been used to calculate the time-average energy of the dot $\langle E\rangle$. We have determined the energy eigenvalues for various combinations of field intensities and used them to compute some of the diagonal and off-diagonal components of linear and nonlinear polarizabilities by the following relations obtained by numerical differentiation. For linear polarizability:

$$\alpha_{xx}\epsilon_x^2 = \frac{5}{2}\langle E(0)\rangle - \frac{4}{3}\left[\langle E(\epsilon_x)\rangle + \langle E(-\epsilon_x)\rangle\right] + \frac{1}{12}\left[\langle E(2\epsilon_x)\rangle + \langle E(-2\epsilon_x)\rangle\right], \tag{14}$$

and a similar expression for $\alpha_{yy}\epsilon_y^2$.

$$\alpha_{xy}\epsilon_x\epsilon_y = \frac{1}{48}\left[E(2\epsilon_x,2\epsilon_y) - E(2\epsilon_x,-2\epsilon_y) - E(-2\epsilon_x,2\epsilon_y) + E(-2\epsilon_x,-2\epsilon_y)\right] - \frac{1}{3}\left[E(\epsilon_x,\epsilon_y) - E(\epsilon_x,-\epsilon_y) - E(-\epsilon_x,\epsilon_y) + E(-\epsilon_x,-\epsilon_x)\right] \tag{15}$$

and a similar expression for computing α_{yx} component.

The components of first nonlinear polarizability (second-order/quadratic hyperpolarizability) are calculated from the following expressions.

$$\beta_{xxx}\epsilon_x^3 = [E(\epsilon_x,0) - E(-\epsilon_x,0)] - \frac{1}{2}[E(2\epsilon_x,0) - E(-2\epsilon_x,0)] \tag{16}$$

and a similar expression is used for computing β_{yyy} component.

$$\beta_{xyy}\ \varepsilon_x\varepsilon_y^2 = \frac{1}{2}\left[E(-\varepsilon_x,\varepsilon_y) - E(\varepsilon_x,\varepsilon_y) + E(-\varepsilon_x,\varepsilon_y) - E(\varepsilon_x,-\varepsilon_y)\right] + \left[E(\varepsilon_x,0) - E(-\varepsilon_x,0)\right] \tag{17}$$

and a similar expression is used for computing β_{yxx} component.

The components of second nonlinear polarizability (third-order/cubic hyperpolarizability) are given by

$$\gamma_{xxxx}\ \epsilon_x^4 = 4[E(\epsilon_x) + E(-\epsilon_x)] - [E(2\epsilon_x) + E(-2\epsilon_x) - 6E(0)], \tag{18}$$

and a similar expression for computing γ_{yyyy} component.

$$\gamma_{xxyy}\ \epsilon_x^2\epsilon_y^2 = 2[E(\epsilon_x) + E(-\epsilon_x)] + 2\left[E(\epsilon_y) + E(-\epsilon_y)\right] - \left[E(\epsilon_x,\epsilon_y) + E(-\epsilon_x,-\epsilon_y) + E(\epsilon_x,-\epsilon_y) + E(-\epsilon_x,\epsilon_y)\right] - 4E(0) \tag{19}$$

and a similar expression for computing γ_{yyxx} component.

3 Results and Discussion

3.1 Linear (α) and Second Nonlinear (γ) Polarizability Components

Figure 2 depicts the profiles of α_{xx} component with variation of n_p for on-center (r_0=0.0 a.u.), near off-center (r_0=28.28 a.u.), and far off-center (r_0=70.71 a.u.) dopant locations, respectively, at three different values of noise strength (μ) viz 0.005 a.u., 0.05 a.u., and 0.5 a.u. The plots reveal that it is the dopant location which influences the α_{xx} profile much more than the noise strength. This is because of the fact that at

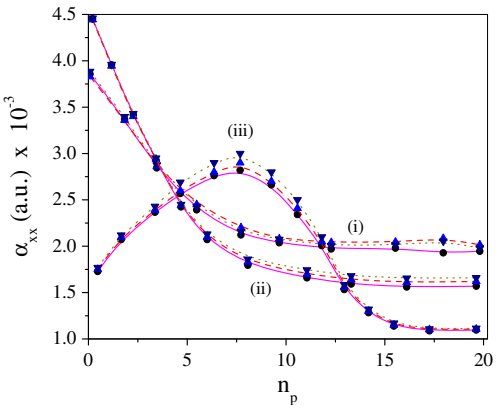

Fig. 2 Plots of α_{xx} vs n_p in the presence of multiplicative noise with (*i*) on-center, (*ii*) near off-center, and (*iii*) far off-center dopants at three different values of μ viz 0.005 a.u., 0.05 a.u., and 0.5 a.u. Note that μ has very little effect on the plots

a particular dopant site the α_{xx} profiles appear quite similar for different values of μ, and their magnitudes also remain nearly unaltered. The profiles undergo a rather prominent change as the dopant location is itself shifted. For on-center (Fig. 2(i)) and near off-center (Fig. 2(ii)) dopants, α_{xx} falls smoothly with an increase in n_p at all noise strengths and finally gets saturated as n_p ~12. However, the magnitude of α_{xx} becomes less for a near off-center dopant than for an on-center one. The α_{xx} profile takes a new appearance for a far off-center dopant (Fig. 2(iii)) when it exhibits distinct maxima at n_p ~8 and finally saturates at n_p ~17 at all values of μ. We could thus infer that the interplay between r_0 and n_p noticeably affects the profile of α_{xx} component. However, the noise strength does not affect the said interplay to any noticeable extent. The other diagonal component α_{yy} evinces almost similar profile. The noise strength becomes very much active in influencing the off-diagonal α_{xy} component. It actively participates as a third member in the already established interplay between r_0 and n_p and brings about more variety in α_{xy} profile. Moreover, we find a reduction (by a factor of ~10^2–10^3) in the magnitude of α_{xy} in comparison with its diagonal counterpart. Figure 3a, b, and c depict the variation of α_{xy} with n_p for on-center, near off-center, and far off-center dopants, respectively, at three different values of μ mentioned before. For an on-center dopant, with μ=0.005 a.u., α_{xy} exhibits a minima at n_p ~8 and finally saturates at n_p ~15 (Fig. 3a(i)). With a higher μ value of 0.05 a.u., the minima becomes 7 quite stretched ranging between n_p ~9 to n_p ~14 and saturation disappears (Fig. 3a(ii)). The minima itself completely vanishes at μ=0.5 a.u. whence α_{xy} falls steadily with n_p up to n_p ~9 beyond which it saturates (Fig. 3a(iii)). For a near off-center dopant the α_{xy} profiles against n_p appear quite similar at all noise strengths though their magnitudes differ noticeably (Fig. 3b). The profiles exhibit an initial steady behavior with increase in *np* followed by a pronounced rise at some typical values of n_p and finally saturate at large n_p values. However, the values of n_p at which the sharp rise occurs and saturation begins depend on noise strength. The said rise occurs at n_p ~8, 7; and 11, with μ= 0.005 a.u., 0.05 a.u., and 0.5 a.u., respectively. On the other hand, the onset of saturation takes place at n_p ~17, 14 and 16, with μ=0.005 a.u., 0.05 a.u., and 0.5 a.u., respectively. The general nature of similar profiles assumes an altogether different appearance for a far off-center dopant (Fig. 3c). Now, we envisage the emergence of maxima in α_{xy} profile at different

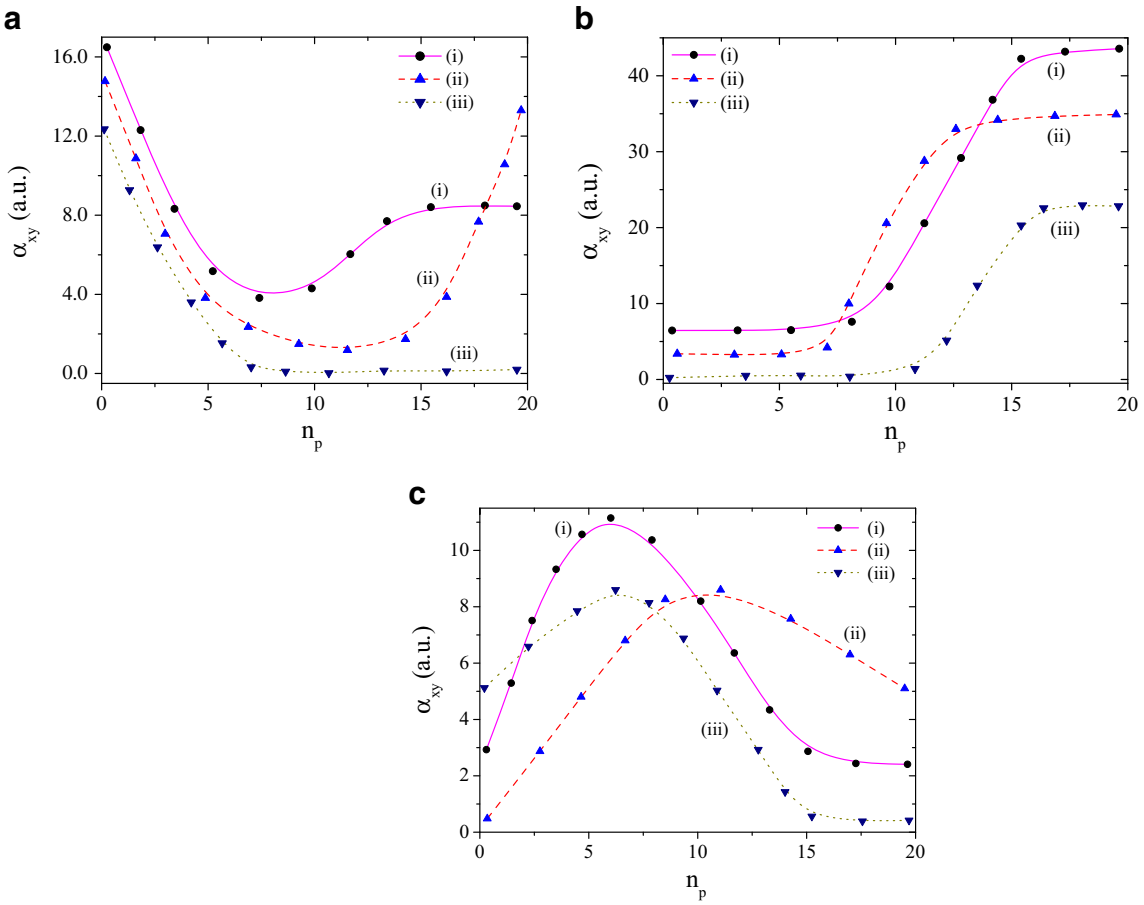

Fig. 3 Plots of α_{xy} component vs n_p in the presence of multiplicative noise: **a** on-center dopant, **b** near off-center dopant, and **c** far off-center dopant, in all the plots (*i*) μ=0.005 a.u., (*ii*) μ=0.05 a.u., and (*iii*) μ=0.5 a.u

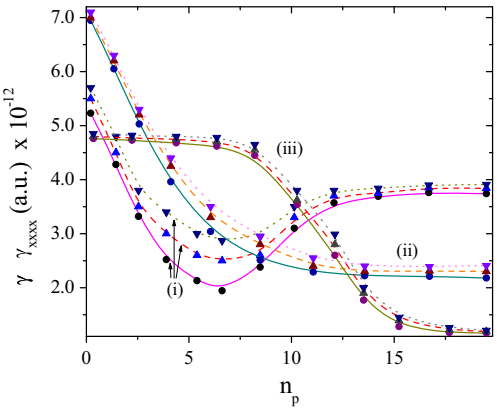

Fig. 4 Plots of γ_{xxxx} vs n_p in the presence of multiplicative noise with (*i*) on-center, (*ii*) near off-center, and (*iii*) far off-center dopants at three different values of μ viz 0.005 a.u., 0.05 a.u., and 0.5 a.u. Note that μ has somewhat observable effect on the plots

values of μ. However, a variation in noise strength simply alters the n_p values at which the said maximization occurs and also the magnitudes of the component. The maximization occurs at n_p ~6, 10, and 6, with μ=0.005 a.u., 0.05 a.u., and 0.5 a.u., respectively. The other off-diagonal component α_{yx} behaves quite similarly. Figure 4 depicts the similar profile for diagonal γ_{xxxx} component at three different dopant sites with three different values of noise strength. Quite similar to α_{xx} plots (Fig. 2), here, also the γ_{xxxx} profiles appear alike at a particular dopant site for different values of μ. However, the separation between several γ_{xxxx} profiles clubbed under a given r_0 now becomes quite prominent depending on different values of μ [Fig. 4]. In the case of α_{xx}, this separation was marginal (Fig. 2). However, as before, a change in the dopant site invariably changes the pattern of the variation of γ_{xxxx} component. For an on-center dopant, γ_{xxxx} exhibits minimization at n_p ~6–7 and saturates later on at n_p ~13 with different values of μ (Fig. 4(i)). In the case of near off-center dopants, γ_{xxxx} declines smoothly with n_p till it undergoes saturation at n_p ~13 at all noise strengths (Fig. 4(ii)). With a far off-center dopant, γ_{xxxx} displays some initial steady behavior up to n_p ~7 followed by a sharp drop until n_p ~18, beyond which saturation emerges (Fig. 4(iii)) at various μ values. The other diagonal component γ_{yyyy} shows high degree of resemblance in its behavior. Figures 5a, b, and c depict the variation of off-diagonal γ_{xxyy} with n_p for on-center, near off-center, and far off-center dopants, respectively, at three different values of μ mentioned before. These plots clearly reveal that, unlike the diagonal component, now the noise strength strongly modulates the γ_{xxyy} profiles along with r_0. Also, its magnitude is diminished by an amount ~10^2–10^3 in comparison with the diagonal counterpart. For an on-center dopant, γ_{xxyy} undergoes minimization at n_p ~8 with μ=0.005 a.u. (Fig. 5a(i)), falls persistently with n_p up to n_p ~12 followed

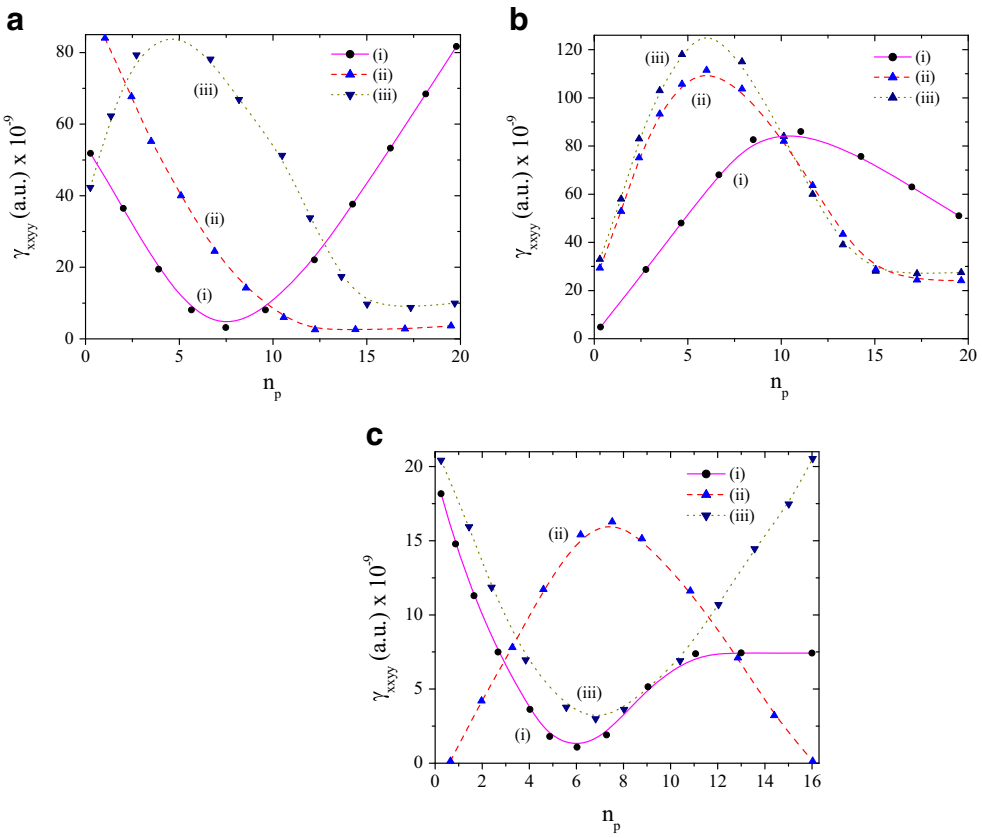

Fig. 5 Plots of γ_{xxyy} component vs n_p in the presence of multiplicative noise: **a** on-center dopant, **b** near off-center dopant, and **c** far off-center dopant, in all the plots (*i*) μ=0.005 a.u., (*ii*) μ=0.05 a.u., and (*iii*) μ=0.5 a.u

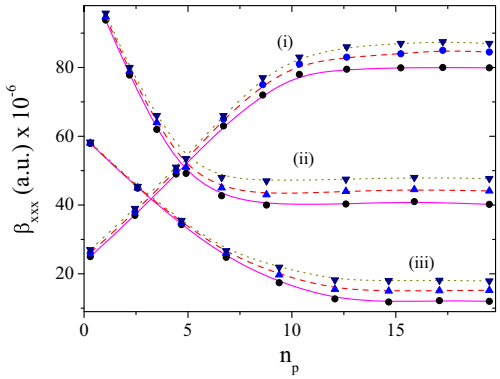

Fig. 6 Plots of β_{xxx} vs n_p in the presence of multiplicative noise with (*i*) on-center, (*ii*) near off-center, and (*iii*) far off-center dopants at three different values of μ viz 0.005 a.u., 0.05 a.u., and 0.5 a.u. Note that μ does not have any appreciable effect on the plots

by saturation with μ=0.05 a.u. (Fig. 5a(ii)), and exhibits maximization and saturation at n_p ~5 and n_p ~16, respectively, with μ=0.005 a.u. (Fig. 5a(iii)). With a dopant introduced into near off-center location, γ_{xxyy} shows maximization at all values of μ (Fig. 5b). However, the magnitude of the component and the n_p values corresponding to maximization differ prominently depending on μ. The said maximization is observed at n_p ~10, 6, and 6 with μ=0.005 a.u., 0.05 a.u., and 0.5 a.u., respectively. γ_{xxyy} depicts minimization for a far off-center dopant at n_p ~6 and 7, with μ= 0.005 a.u. and 0.5 a.u., respectively (Fig. 5c). Moreover, in the previous case, it also exhibits saturation at n_p ~12. However, with μ=0.05 a.u., we observe a maximization at n_p ~7. The other off-diagonal component, i.e., γ_{yyxx} does not display any new feature.

3.2 First Nonlinear (β) Polarizability Components

The application of multiplicative noise lifts the symmetry of the system and helps in the emergence of β. Figure 6 represents the profiles of diagonal β_{xxx} component as a function of n_p for on-center, near off-center, and far on-center dopants at different values of μ. From the figure, it is evident that for a particular dopant site the noise strength does not appreciably change the β_{xxx} profile. A change in dopant site, however, noticeably affects the pattern as well as the magnitude of β_{xxx} component. For an on-center dopant, β_{xxx} increases steadily with n_p up to n_p ~13 and saturates thereafter at all noise strengths (Fig. 6(i)). For a near off-center dopant, β_{xxx} drops persistently till n_p ~9 beyond which it saturates at all μ (Fig. 6(ii)). With a far off-center dopant, the overall pattern remains somewhat similar to that of near off-center dopant with the difference that now β_{xxx} falls more slowly and the saturation occurs at n_p ~13 (Fig. 6(iii)). The other diagonal component β_{yyy} shows similar behavior. We have found a stronger influence of noise strength even for the off-diagonal β components. Figure 7a–c delineates the similar profiles for the off-diagonal β_{xyy} component for on-center, near on-center, and far off-center dopants, respectively, for different values of μ. For an on-center dopant, with μ=0.005 a.u., β_{xyy} exhibits minimization at n_p ~12 (Fig. 7a(i)). The similar plot exhibits maximization and

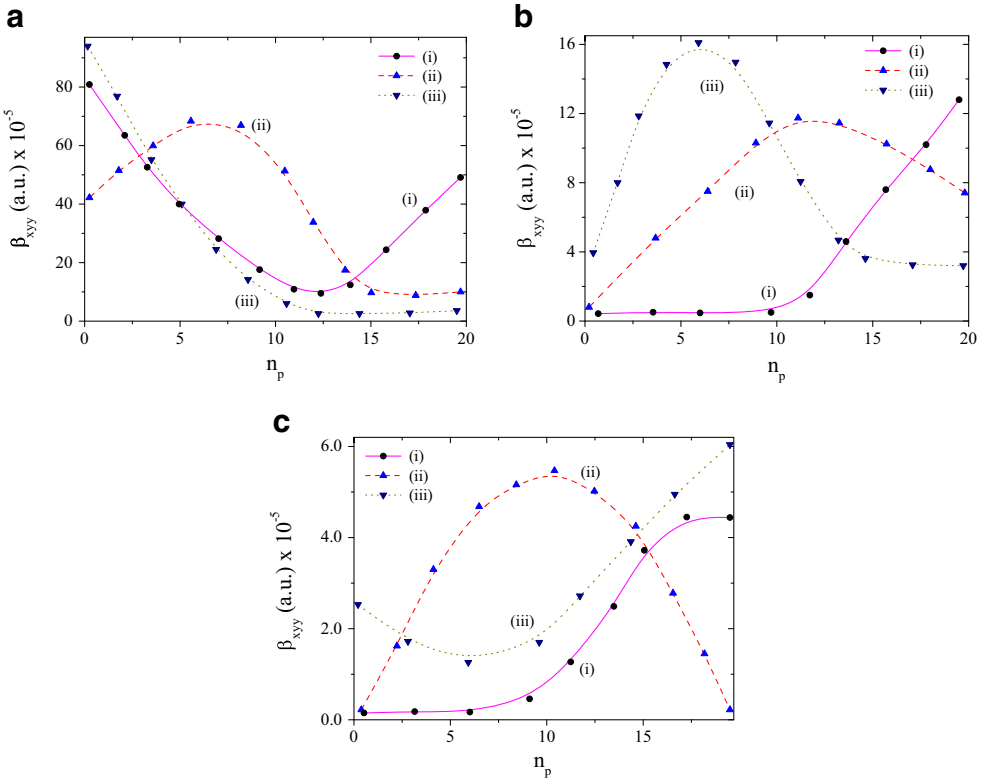

Fig. 7 Plots of β_{xyy} component vs n_p in the presence of multiplicative noise: **a** on-center dopant, **b** near off-center dopant, and **c** far off-center dopant, in all the plots (*i*) μ=0.005 a.u., (*ii*) μ=0.05 a.u., and (*iii*) μ=0.5 a.u

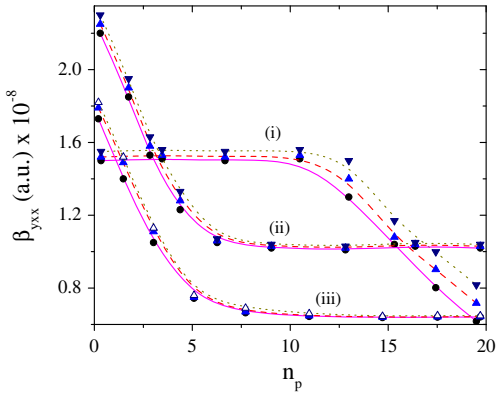

Fig. 8 Plots of β_{yxx} vs n_p in the presence of multiplicative noise with (*i*) on-center, (*ii*) near off-center, and (*iii*) far off-center dopants at three different values of μ viz 0.005 a.u., 0.05 a.u., and 0.5 a.u. Note that μ does not have any appreciable effect on the plots

onset of saturation at n_p ~6 and n_p ~15, respectively, with μ= 0.05 a.u. (Fig. 7a(ii)). The scenario changes with μ=0.5 a.u. while β_{xyy} decreases steadily up to n_p ~12 and saturation begins thereafter (Fig. 7a(iii)). In the case of a near off-center dopant, β_{xyy} displays a nearly fixed value up to n_p ~10 and then rises prominently (Fig. 7b(i)) with μ=0.005 a.u. With μ=0:05 a.u., the said component exhibits a weak maxima at n_p ~12 (Fig. 7b(ii)). With still higher value of μ=0.5 a.u., we find a well-defined maxima in β_{xyy} profile at n_p ~6 and saturation that commences at n_p ~17 (Fig. 7b(iii)). For a far off-center dopant and with μ=0.005 a.u., β_{xyy} exhibits a nearly steady behavior up to n_p ~7; after which, it rises noticeably and finally saturates at n_p ~17 (Fig. 7c(i)). With μ=0.05 a.u., we observe prominent maximization in β_{xyy} at n_p ~10 (Fig. 7c(ii)). With μ=0.5 a.u., a feeble minimization in β_{xyy} at n_p ~6 has been observed (Fig. 7c(iii)). It is quite interesting as well as unexpected to find that the other off-diagonal β component viz β_{yxx} does not exhibit any significant dependence on noise strength. However, the dopant location continues to influence the polarizability profile as before. Figure 8 displays the profile of β_{yxx} vs n_p for on-center (Fig. 8(i)), near off-center (Fig. 8(ii)), and far off-center dopants (Fig. 8(iii)), respectively, for different values of μ. With an on-center dopant, β_{yxx} exhibits constancy up to n_p ~9 beyond which it decreases monotonically at all μ. β_{yxx} profiles resemble each other for near and far off-center dopants at all values of noise strength. In both the cases, β_{yxx} falls steadily with n_p up to n_p ~7 (for near off-center dopant) and n_p ~8 (for far off-center dopant) and then saturates. A steady drop in the magnitude of β_{yxx} with gradual shift of dopant from on to more and more off-center locations has also been observed owing to continual shrinkage in dot-impurity overlap. The reason behind the pronounced effect of noise strength on β_{xyy} component and its inactiveness towards β_{yxx} component can be realized by a close look at Eq. 3. It reveals a greater confinement in the *y*-direction compared with the *x*-direction. Thus, the *y*-direction suffers greater dot-impurity repulsive force than the *x*-direction. Since β_{xyy} component enjoys a greater share of *y*-directional influence than the β_{yxx} component, the former is subjected to a more severe dot-impurity repulsive interaction than the latter. Such kind of repulsive interaction makes the system already dispersed and favors prominent manifestation of influence of noise strength on β_{xyy}, which is not so in case of β_{yxx}.

It thus comes out that the dopant location, the number of pulses, and the noise strength affect the polarizability profiles with sufficient delicacy. Particularly, the role played by the dopant site in the present work runs in harmony with the outcomes of other notable works which highlight the contribution of dopant location in designing various properties of mesoscopic systems. In this context the works of Sadeghi and Avazpour [4, 5], Yakar et al. [7], Xie [9], Karabulut and Baskoutas [25], Khordad and Bahramiyan [30], and Baskoutas and his co-workers [32] merit mention.

4 Conclusions

A few diagonal and off-diagonal components of linear, first nonlinear, and second nonlinear polarizabilities of impurity doped quantum dots have been examined under the influence of a pulsed field and in the presence of multiplicative Gaussian white noise. The number of pulses delivered to the system, the dopant location, and the noise strength manifestly fabricate the polarizability profiles. Whereas a variation in n_p directly controls the energy input from the external field, a varying r_0 modulates the spatial distribution of energy levels internally through different degrees of dot-impurity interaction. On the other hand, a variation in noise strength regulates the overall dispersive character of the system. It has been observed that the influence of noise strength becomes more pronounced for the off-diagonal polarizability components than their diagonal counterparts. The above observation looses its generality for the off-diagonal β_{yxx} component which does not get much influenced by a variation of noise strength. The study reveals that the simultaneous application of pulsed field and multiplicative noise can design some authentic modes of accomplishing enhanced, maximized, and often stable linear and nonlinear polarizabilities of doped QD which could be important in the arena of noise-driven optical properties of these systems.

References

1. B. Gülveren, Ü. Atav, M. Şahin, M. Tomak, A parabolic quantum dot with *N* electrons and an impurity. Physica E **30**, 143–149 (2005)
2. H. Taş, M. Şahin, The electronic properties of core/shell/well/shell spherical quantum dot with and without a hydrogenic impurity, J. Appl. Phys. 111, 083702 (8 pages) (2012)
3. S. Baskoutas, A.F. Terzis, E. Voutsinas, Binding energy of donor states in a quantum dot with parabolic confinement. J. Comput. Theor. Nanosci. **1**, 317–321 (2004)

4. E. Sadeghi, A. Avazpour, Binding energy of an off-center donor impurity in ellipsoidal quantum dot with parabolic confinement potential. Physica B **406**, 241–244 (2011)
5. E. Sadeghi, Impurity binding energy of excited states in spherical quantum dot. Physica E **41**, 1319–1322 (2009)
6. M. Barati, M. R. K Vahdani, G. Rezaei, Lower-lying states of hydrogenic impurity in lens-shaped and semi-lens-shaped quantum dots, J. Phys.:Condensed Matter 19, 136208 (14 pages) (2007)
7. Y. Yakar, B. Çakír, Ö. A, Off-center hydrogenic impurity in spherical quantum dot with parabolic potential. Superlattice Microst **60**, 389–397 (2013)
8. S. Akgül, M. Şahin, K. Köksal, A detailed investigation of the electronic properties of a multi-layer spherical quantum dot with a parabolic confinement. J. Lumin. **132**, 1705–1713 (2012)
9. W. Xie, Binding energy of an off-center hydrogenic donor in a spherical Gaussian quantum dot. Physica B **403**, 2828–2831 (2008)
10. M.R.K. Vahdani, G. Rezaei, Linear and nonlinear optical properties of a hydrogenic donor in lens-shaped quantum dots. Phys. Lett. A **373**, 3079–3084 (2009)
11. G. Rezaei, M.R.K. Vahdani, B. Vaseghi, Nonlinear optical properties of a hydrogenic impurity in an ellipsoidal finite potential quantum dot. Curr. Appl. Phys. **11**, 176–181 (2011)
12. W. Xie, Impurity effects on optical property of a spherical quantum dot in the presence of an electric field. Physica B **405**, 3436–3440 (2010)
13. I. Karabulut, S. Baskoutas, Linear and nonlinear optical absorption coefficients and refractive index changes in spherical quantum dots: effects of impurities, electric field, size, and optical intensity, J. Appl. Phys. 103, 073512 (5 pages)(2008)
14. Y. Yakar, B. Çakir, A. Özmen, Calculation of linear and nonlinear optical absorption coefficients of a spherical quantum dot with parabolic potential, Optics Commun. 283, 1795-1800 (2010)
15. T. Chen, W. Xie, S. Liang, Optical and electronic properties of a two-dimensional quantum dot with an impurity. J. Lumin. **139**, 64–68 (2013)
16. M. Şahin, Third-order nonlinear optical properties of a one- and two-electron spherical quantum dot with and without a hydrogenic impurity, J. Appl. Phys. 106, 063710 (8 pages) (2009)
17. B. Çakir, Y. Yakar, A. Özmen, M. Özgür Sezer, M. Şahin, Linear and nonlinear optical absorption coefficients and binding energy of a spherical quantum dot. Superlattice Microst **47**, 556–566 (2010)
18. B. Çakir, Y. Yakar, A. Özmen, Refractive index changes and absorption coefficients in a spherical quantum dot with parabolic potential. J. Lumin. **132**, 2659–2664 (2012)
19. B. Çakir, Y. Yakar, A. Özmen, Linear and nonlinear optical absorption coefficient of two-electron spherical quantum dot with parabolic potential. Physica B **458**, 138–143 (2015)
20. W. Xie, Nonlinear optical properties of a hydrogenic donor quantum dot. Phys. Lett. A **372**, 5498–5500 (2008)
21. S. Baskoutas, E. Paspalakis, A. F. Terzis, Effects of excitons in nonlinear optical rectification in semiparabolic quantum dots, Phys. Rev. B 74, 153306 (4 pages) (2006).
22. Z. Zeng, C.S. Garoufalis, A.F. Terzis, S. Baskoutas, Linear and nonlinear optical properties of ZnS/ZnO core shell quantum dots: effect of shell thickness, impurity, and dielectric environment. J. Appl. Phys. **114**, 023510 (2013)
23. A. John Peter, Polarizabilities of shallow donors in spherical quantum dots with parabolic confinement. Phys. Lett. A **355**, 59–62 (2006)
24. W. Xie, Linear and nonlinear optical properties of a hydrogenic donor in spherical quantum dots. Physica B **403**, 4319–4322 (2008)
25. I. Karabulut, S. Baskoutas, Second and third harmonic generation susceptibilities of spherical quantum dots: effects of impurities, electric field and size. J. Comput. Theor. Nanosci. **6**, 153–156 (2009)
26. K.M. Kumar, A.J. Peter, C.W. Lee, Optical properties of a hydrogenic impurity in a confined $Zn_{1-x}Cd_xSe/ZnSe$ quantum dot. Superlattice Microst **51**, 184–193 (2012)
27. A. Tiutiunnyk, V. Tulupenko, M.E. Mora-Ramos, E. Kasapoglu, F. Ungan, H. Sari, I. Sökmen, C.A. Duque, Electron-related optical responses in triangular quantum dots. Physica E **60**, 127–132 (2014)
28. W. Xie, Nonlinear optical properties of a hydrogenic donor quantum dot. Phys. Lett. A **372**, 5498–5500 (2008)
29. S. Yilmaz, M. Şahin, Third-order nonlinear absorption spectra of an impurity in a spherical quantum dot with different confining potential. Phys. Status Solidi B **247**, 371–374 (2010)
30. R. Khordad, H. Bahramiyan, Impurity position effect on optical properties of various quantum dots. Physica E **66**, 107–115 (2015)
31. W. Xie, S. Liang, Optical properties of a donor impurity in a two-dimensional quantum pseudodot. Physica B **406**, 4657–4660 (2011)
32. S. Baskoutas, E. Paspalakis, A. F. Terzis, Electronic structure and nonlinear optical rectification in a quantum dot: effects of impurities and external electric field, J. Phys:Cond. Mat. 19, 395024 (9- pages) (2007)
33. N.V. Lien, N.M. Trinh, Electric field effects on the binding energy of hydrogen impurities in quantum dots with parabolic confinements. J. Phys.Condens. Mater **13**, 2563–2571 (2001)
34. G. Murillo, N. Porras-Montenegro, Effects of an electric field on the binding energy of a donor impurity in a spherical GaAs(Ga, Al)As quantum dot with parabolic confinement. Phys. Status Solidi B **220**, 187–190 (2000)
35. M. Kirak, S. Yilmaz, M. Sahin, M. Gençasian, The electric field effects on the binding energies and the nonlinear optical properties of a donor impurity in a spherical quantum dot. J. Appl. Phys. **109**, 094309 (2011)
36. C.M. Duque, M.E. Mora-Ramos, C.A. Duque, Hydrostatic pressure and electric field effects and nonlinear optical rectification of confined excitons in spherical quantum dots. Superlattice Microst **49**, 264–268 (2011)
37. C.M. Duque, M.G. Barseghyan, C.A. Duque, Hydrogenic impurity binding energy in vertically coupled $GaAsGa_{1-x}Al_xAs$ quantum-dots under hydrostatic pressure and applied electric field. Physica B **404**, 5177–5180 (2009)
38. M.G. Barseghyan, A.A. Kirakosyan, C.A. Duque, Donor-impurity related binding energy and photoionization cross-section in quantum dots: electric and magnetic field effects. Eur. Phys. J. B **72**, 521–529 (2009)
39. C.M. Duque, M.G. Barseghyan, C.A. Duque, Donor impurity in vertically-coupled quantum dots under hydrostatic pressure and applied electric field. Eur. Phys. J. B **73**, 309–319 (2010)
40. C.M. Duque, M.E. Mora-Ramos, C.A. Duque, Hydrostatic pressure and electric field effects and nonlinear optical rectification of confined excitons in spherical quantum dots. Superlattice Microst **49**, 264–268 (2011)
41. M.E. Mora-Ramos, C.A. Duque, E. Kasapoglu, H. Sari, I. Sökmen, Study of direct and indirect exciton states in $GaAsGa_{1-x}Al_xAs$ quantum dots under the effects of intense laser field and applied electric field. Eur. Phys. J. B **85**, 312 (2012)
42. M. Narayanan, A. John Peter, Electric field induced exciton binding energy and its non-linear optical properties in a narrow $InSb/InGa_xSb_{1-x}$ quantum dot. Superlattice Microst **51**, 486–496 (2012)
43. S.Y. López, N. Porras-Montenegro, C.A. Duque, Excitons in coupled quantum dots: hydrostatic pressure and electric field effects. Phys Status Solidi B **246**, 630–634 (2009)
44. E. Kasapoglu, F. Ungan, H. Sari, I. Sökmen, M.E. Mora-Ramos, C.A. Duque, Donor impurity states and related optical responses in triangular quantum dots under applied electric field. Superlattice Microst **73**, 171–184 (2014)
45. E. Sadeghi, Electric field and impurity effects on optical property of a three-dimensional quantum dot: a combinational potential scheme. Superlattice Microst **50**, 331–339 (2011)

46. W. Xie, Q. Xie, Electric field effects of hydrogenic impurity states in a disc-like quantum dot. Physica B **404**, 1625–1628 (2009)
47. S. Liang, W. Xie, X. Li, H. Shen, Photoionization and binding energy of a donor impurity in a quantum dot under an electric field: effects of the hydrostatic pressure and temperature. Superlattice Microst **49**, 623–631 (2011)
48. B. Çakir, Y. Yakar, A. Özmen, Calculation of oscillator strength and the effects of electric field on energy states, static and dynamic polarizabilities of the confined hydrogen atom. Optics Commun. B **311**, 222–228 (2013)
49. J. Ganguly, M. Ghosh, Influence of Gaussian white noise on the frequency-dependent linear polarizability of doped quantum dot. Chem. Phys. **438**, 75–82 (2014)
50. J. Ganguly, M. Ghosh, Influence of Gaussian white noise on the frequency-dependent first nonlinear polarizability of doped quantum dot, J. Appl. Phys. 115, 174313 (10 pages) (2014)
51. J. Ganguly, M. Ghosh, Exploring static and frequency-dependent third nonlinear polarizability of doped quantum dots driven by Gaussian white noise. Phys Status Solidi B **252**, 289–297 (2015)
52. A. Gharaati, R. Khordad, A new confinement potential in spherical quantum dots: modified Gaussian potential. Superlattice Microst **48**, 276–287 (2010)
53. R. Khordad, Use of modified Gaussian potential to study an exciton in a spherical quantum dot. Superlattice Microst **54**, 7–15 (2013)
54. J. Adamowski, A. Kwasniowski, B. Szafran, LO-phonon-induced screening of electron–electron interaction in D^- centres and quantum dots. J. Phys. Condens. Matter. **17**, 4489–4500 (2005)
55. B. Szafran, S. Bednarek, J. Adamowski, Parity symmetry and energy spectrum of excitons in coupled self-assembled quantum dots, Phys. Rev. B 64, 125301 (10- pages) (2001)